

Subspace Constrained Variational Bayesian Inference for Structured Compressive Sensing with a Dynamic Grid

An Liu, *Senior Member, IEEE*, Yufan Zhou, and Wenkang Xu

Abstract—We investigate the problem of recovering a structured sparse signal from a linear observation model with an uncertain dynamic grid in the sensing matrix. The state-of-the-art expectation maximization based compressed sensing (EM-CS) methods, such as turbo compressed sensing (Turbo-CS) and turbo variational Bayesian inference (Turbo-VBI), have a relatively slow convergence speed due to the double-loop iterations between the E-step and M-step. Moreover, each inner iteration in the E-step involves a high-dimensional matrix inverse in general, which is unacceptable for problems with large signal dimensions or real-time calculation requirements. Although there are some attempts to avoid the high-dimensional matrix inverse by majorization minimization, the convergence speed and accuracy are often sacrificed. To better address this problem, we propose an alternating estimation framework based on a novel subspace constrained VBI (SC-VBI) method, in which the high-dimensional matrix inverse is replaced by a low-dimensional subspace constrained matrix inverse (with the dimension equal to the sparsity level). We further prove the convergence of the SC-VBI to a stationary solution of the Kullback-Leibler divergence minimization problem. Simulations demonstrate that the proposed SC-VBI algorithm can achieve a much better tradeoff between complexity per iteration, convergence speed, and performance compared to the state-of-the-art algorithms.

Index Terms—Subspace constrained variational Bayesian inference (SC-VBI), structured sparse signal recovery, dynamic grid.

I. INTRODUCTION

The problem of structured compressive sensing (CS) with dynamic grids has attracted a lot of research due to its wide applications in signal processing and wireless communications [1]–[3]. The goal of this problem is to recover a structured sparse signal $\mathbf{x} = [x_1, \dots, x_N]^T \in \mathbb{C}^{N \times 1}$ from significantly fewer measurements $\mathbf{y} \in \mathbb{C}^{M \times 1}$ (i.e., $M \ll N$) under the following linear observation model:

$$\mathbf{y} = \mathbf{A}(\boldsymbol{\theta}) \mathbf{x} + \mathbf{w}, \quad (1)$$

where $\mathbf{A}(\boldsymbol{\theta}) \in \mathbb{C}^{M \times N}$ is the sensing matrix with dynamic grid parameters $\boldsymbol{\theta}$, $\mathbf{w} \in \mathbb{C}^{M \times 1}$ is the noise vector with independent Gaussian entries.

In the standard CS problem, $\boldsymbol{\theta}$ is chosen to be a pre-determined fixed grid and \mathbf{x} is an i.i.d. sparse signal. However, in practice, the true grid parameters $\boldsymbol{\theta}$ usually do not lie exactly on the pre-determined fixed grid points. For example, in massive MIMO channel estimation, the grid parameters

$\boldsymbol{\theta}$ correspond to the angles of the active channel paths. If we use a fixed angle grid, the estimation accuracy of the angles $\boldsymbol{\theta}$ will be limited by the grid resolution, which will also cause energy leakage and degrade the channel estimation performance [1]. Future 6G wireless systems are expected to also provide sensing services, and it is important to achieve “super resolution” estimation of the angle/delay parameters to realize high-accuracy sensing and localization [4], [5]. In this case, we also need to adjust the grid to achieve more accurate estimation of the grid parameters $\boldsymbol{\theta}$ and alleviate the energy leakage effect. Moreover, in many practical applications, the sparse signal \mathbf{x} usually has structured sparsity that cannot be modeled easily by an i.i.d. prior. Therefore, it is very important to consider the structured CS problem with a dynamic grid.

The state-of-the-art methods to solve the structured CS problem with a dynamic grid are those expectation maximization based compressed sensing (EM-CS) methods, which iterates between the E-step and M-step. In the E-step, the turbo approach is often applied to compute a Bayesian estimation of \mathbf{x} with a structured sparse prior by exchanging extrinsic messages between two modules until convergence. Specifically, one module (say Module A) performs Bayesian inference over the observation model and another module (say Module B) performs message passing over the structured sparse prior. Various Turbo-based algorithms have been proposed for the E-step, such as turbo approximate message passing (Turbo-AMP) [6], turbo compressive sensing (Turbo-CS) [7], [8], and turbo variational Bayesian inference (Turbo-VBI) [9], [10], whose Module A is the AMP estimator, the linear minimum mean square error (LMMSE) estimator, and the VBI estimator, respectively. In the M-step, a surrogate function of the likelihood function for the grid parameters is firstly constructed from the Bayesian estimation of \mathbf{x} obtained in the E-step and then the gradient ascent method is used to update the dynamic grid parameters by maximizing the surrogate function.

Although the EM-CS methods are shown to achieve a good performance in various applications [3], [8], [11], [12], there are still several drawbacks. Firstly, the EM-CS methods contain two-loop of iterations, namely, the inner iterations in the E-step between Module A and Module B and the outer iteration between the E-step and M-step. Secondly, the Module A in the E-step involves an N -dimensional matrix inverse in general, which has a high computational complexity for large-scale problems (i.e., when N is large). There are a few exceptions, e.g., when the sensing matrix $\mathbf{A}(\boldsymbol{\theta})$ has i.i.d. entries or

An Liu, Yufan Zhou, and Wenkang Xu are with the College of Information Science and Electronic Engineering, Zhejiang University, Hangzhou 310027, China (email: anliu@zju.edu.cn).

is partially orthogonal (i.e., the rows of the sensing matrix are mutually orthogonal), the matrix inverse can be avoided in the E-step of Turbo-AMP and Turbo-CS, respectively. However, this is not the case for many practical applications, especially when the sensing matrix contains dynamic grid parameters θ . It is impossible for the sensing matrix $\mathbf{A}(\theta)$ to satisfy the above good properties for different values of θ . Finally, the M-step is based on maximizing a surrogate likelihood function of θ , making it difficult to choose a good step size using e.g., backtrack line search, since a good step size for the surrogate likelihood function is not necessarily good for the true likelihood function (as observed in many experiments). As such, the EM-CS methods often need a relatively large number of inner iterations to converge to a good accuracy and the complexity per inner iteration is also high especially for large-scale problems.

Recently, there are a few works attempting to avoid the high-dimensional matrix inverse. For example, in [13], [14], the authors proposed an inverse-free VBI (IF-VBI) algorithm that avoids the matrix inverse by maximizing a relaxed evidence lower bound (ELBO). In a very recent work [15], an inverse-free successive linear approximation VBI (IFSLA-VBI) method was developed, where the matrix inverse is avoided by solving a quadratic minimization problem based on the majorization minimization (MM) framework. Although the MM methods in [13]–[15] completely avoided the matrix inverse, they added another loop of MM iterations to approximate the high-dimensional matrix inverse and thus the overall convergence speed is expected to be slow. Moreover, the IF-VBI method needs a singular value decomposition (SVD) operation additionally in order to construct the ELBO, and the IFSLA-VBI method adds some additional calculations due to the successive linear expansion of the observation model and consideration of Bayesian inference for the non-linear dynamic parameters θ .

Another line of works have proposed an atomic norm minimization approach to achieve gridless CS. In [16], [17], the authors showed that the sparse signal and sensing parameters can be exactly recovered with high probability via atomic norm minimization, provided the sensing parameters are well separated. However, atomic norm minimization involves semi-definite programming, which has a much higher complexity than the EM-CS method. Moreover, it is difficult to incorporate the more complicated structured sparsity in the framework of atomic norm minimization.

In this paper, we propose an alternating estimation framework based on a novel subspace constrained VBI (SC-VBI) method to overcome the drawbacks of the existing methods. The main contributions are summarized below.

- **An alternating estimation framework:** We propose an alternating estimation framework that iterates among the SC-VBI module, the grid estimation (GE) module, and the structured sparse inference (SSI) module. For fixed grid parameter θ and extrinsic message from the SSI module, the SC-VBI module computes a Bayesian estimation of \mathbf{x} based on the observation model. For fixed MMSE estimator of \mathbf{x} output from the SC-VBI module, the GE module refines the dynamic grid by directly

maximizing the likelihood function based on the gradient ascent method with backtracking line search. Finally, for fixed extrinsic message from the SC-VBI module, the SSI module performs sum-product message passing over the structured sparse prior to exploit the specific sparse structures in practical applications.

- **Subspace constrained VBI (SC-VBI):** The key motivation for SC-VBI comes from the following observation. Suppose the sparsity level of \mathbf{x} is $S \ll N$. If we know the support of the sparse signal (i.e., the index set \mathcal{S} to indicate the locations of the non-zero elements in the sparse signal \mathbf{x}), we can simply omit the zero elements in \mathbf{x} and perform LMMSE to recover \mathbf{x} with only a S -dimensional matrix inverse. Therefore, let \mathbf{W}_x denote the N -dimensional matrix that needs to be inverted in the VBI. We can first estimate the support $\hat{\mathcal{S}}$ and then set all off-diagonal elements that are not in the rows/columns indexed by $\hat{\mathcal{S}}$ to zero. Then the resulting matrix inverse \mathbf{W}_x^{-1} can be completed by only calculating the inverse of a S -dimensional sub-matrix of \mathbf{W}_x restricted to the subspace indexed by $\hat{\mathcal{S}}$. To fix the error caused by using the estimated support $\hat{\mathcal{S}}$ instead of the true support \mathcal{S} , we further apply $B_x \geq 1$ gradient update to refine the posterior mean of \mathbf{x} . Finally, a robust design is also introduced to ensure the fast convergence of the SC-VBI.
- **Theoretical Convergence Analysis for SC-VBI:** Despite the error caused by using the estimated support $\hat{\mathcal{S}}$ and a finite number of gradient updates, we show that the proposed SC-VBI converges to a stationary solution of the original VBI problem (i.e., the KL-divergence (KLD) minimization problem).

The rest of the paper is organized as follows. In Section II, we introduce a three-layer sparse prior model and formulate the structured CS problem with a dynamic grid. The proposed alternating estimation framework is presented in Section III. The SC-VBI algorithm and its convergence analysis are presented in Section IV. The proposed algorithm are applied to solve a massive MIMO channel estimation problem in Section V. Finally, the conclusion is given in Section VI.

Notation: Lowercase boldface letters denote vectors and uppercase boldface letters denote matrices. $(\cdot)^{-1}$, $(\cdot)^T$, $(\cdot)^H$, $\|\cdot\|$, and $\langle \cdot \rangle$ are used to represent the inverse, transpose, conjugate transpose, ℓ_2 -norm, and expectation operations, respectively. \mathbf{I}_M denotes the $M \times M$ dimensional identity matrix. Let $\Re\{ \cdot \}$ denote the real part of the complex argument. For a vector $\mathbf{x} \in \mathbb{C}^N$ and a given index set $\mathcal{S} \subseteq \{1, \dots, N\}$, $|\mathcal{S}|$ denotes its cardinality, $\mathbf{x}_{\mathcal{S}} \in \mathbb{C}^{|\mathcal{S}| \times 1}$ denotes the subvector consisting of the elements of \mathbf{x} indexed by the set \mathcal{S} . $\text{diag}(\mathbf{x})$ denotes a block diagonal matrix with \mathbf{x} as the diagonal elements. $\mathcal{CN}(\mathbf{x}; \boldsymbol{\mu}, \boldsymbol{\Sigma})$ represents a complex Gaussian distribution with mean $\boldsymbol{\mu}$ and covariance matrix $\boldsymbol{\Sigma}$. $\Gamma(x; a, b)$ represents a Gamma distribution with shape parameter a and rate parameter b . Finally, $x = \Theta(a)$ for $a > 0$ denotes that $\exists k_1, k_2 > 0$, such that $k_2 \cdot a \leq x \leq k_1 \cdot a$.

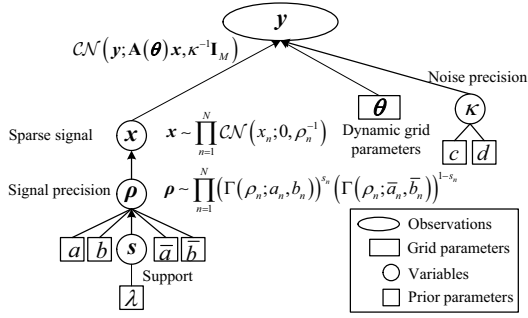


Figure 1: Three-layer hierarchical structured sparse prior.

II. STRUCTURED SPARSITY MODEL AND PROBLEM FORMULATION

A. Three-layer Sparse Prior Model

The probability model for structured sparsity provides the foundation for exploiting the specific sparse structures. A good sparse probability model should satisfy the following criteria: it is flexible to capture the sparse structure of the sparse signal; it is robust w.r.t. the imperfect prior information in practice; and it is tractable to enable low-complexity and high-performance algorithm design. In the following, we shall briefly introduce the three-layer sparse prior model proposed in [9], which has been verified to meet all these criteria in [9], [10].

In the three-layer sparse prior, a support vector $\mathbf{s} \triangleq [s_1, \dots, s_N]^T \in \{0, 1\}^N$ is introduced to indicate whether the n -th element x_n in \mathbf{x} is active ($s_n = 1$) or inactive ($s_n = 0$). Specifically, let $\boldsymbol{\rho} = [\rho_1, \dots, \rho_N]^T$ denote the precision vector of \mathbf{x} (i.e., $1/\rho_n$ denotes the variance of x_n). Then the joint distribution of \mathbf{x} , $\boldsymbol{\rho}$, and \mathbf{s} can be expressed as

$$p(\mathbf{x}, \boldsymbol{\rho}, \mathbf{s}) = \underbrace{p(\mathbf{s})}_{\text{Support}} \underbrace{p(\boldsymbol{\rho} | \mathbf{s})}_{\text{Precision}} \underbrace{p(\mathbf{x} | \boldsymbol{\rho})}_{\text{Sparse signal}}, \quad (2)$$

as illustrated in Fig. 1. In the following, we detail the probability model for each variable.

The prior distribution $p(\mathbf{s})$ of the support vector is used to capture the structured sparsity in specific applications. For example, to capture an independent sparse structure, we can set

$$p(\mathbf{s}) = \prod_{n=1}^N (\lambda_n)^{s_n} (1 - \lambda_n)^{1-s_n}, \quad (3)$$

where λ_n is the sparsity ratio. In [9], $p(\mathbf{s})$ is chosen to be a Markov chain to model the clustered scattering environment in massive MIMO channel.

The conditional probability $p(\boldsymbol{\rho} | \mathbf{s})$ is given by

$$p(\boldsymbol{\rho} | \mathbf{s}) = \prod_{n=1}^N (\Gamma(\rho_n; a_n, b_n))^{s_n} (\Gamma(\rho_n; \bar{a}_n, \bar{b}_n))^{1-s_n}, \quad (4)$$

where $\Gamma(\rho; a, b)$ is a Gamma hyper-prior with shape parameter a and rate parameter b . When $s_n = 1$, the variance $1/\rho_n$ of x_n is $\Theta(1)$, and thus the shape and rate parameters a_n, b_n should be chosen such that $\frac{\bar{a}_n}{\bar{b}_n} = \mathbb{E}[\rho_n] = \Theta(1)$. On the other hand, when $s_n = 0$, x_n is close to zero, and thus the

shape and rate parameters \bar{a}_n, \bar{b}_n should be chosen to satisfy $\frac{\bar{a}_n}{\bar{b}_n} = \mathbb{E}[\rho_n] \gg 1$.

The conditional probability $p(\mathbf{x} | \boldsymbol{\rho})$ for the sparse signal is assumed to have a product form $p(\mathbf{x} | \boldsymbol{\rho}) = \prod_{n=1}^N p(x_n | \rho_n)$ and each $p(x_n | \rho_n)$ is modeled as a complex Gaussian prior distribution

$$p(x_n | \rho_n) = \mathcal{CN}(x_n; 0, \rho_n^{-1}), \forall n = 1, \dots, N. \quad (5)$$

B. Structured CS Problem Formulation with a Dynamic Grid

Recall the CS model with a dynamic grid in the sensing matrix

$$\mathbf{y} = \mathbf{A}(\boldsymbol{\theta}) \mathbf{x} + \mathbf{w}, \quad (6)$$

where $\mathbf{w} \in \mathbb{C}^{M \times 1}$ is the noise vector with independent Gaussian entries $w_m \sim \mathcal{CN}(w_m; 0, \kappa^{-1})$. We employ a Gamma distribution with parameters c and d to model the noise precision, i.e.,

$$p(\kappa) = \Gamma(\kappa; c, d). \quad (7)$$

The Gamma distribution can capture the practical distribution of the noise precision well and is a conjugate of the Gaussian prior. Therefore, it has been widely used to model the noise precision in Bayesian inference [1], [9], [10], [13], [18].

Given the observation \mathbf{y} , we aim at computing a Bayesian estimation of the sparse signal \mathbf{x} and support \mathbf{s} , i.e., the posterior $p(\mathbf{x} | \mathbf{y})$ and $p(\mathbf{s} | \mathbf{y})$, and the maximum likelihood estimation (MLE) of grid parameters $\boldsymbol{\theta}$, i.e., $\arg\max \ln p(\boldsymbol{\theta} | \mathbf{y})$.

Note that we can also obtain an MMSE estimate of \mathbf{x} and a MAP estimate of \mathbf{s} from the Bayesian estimation $p(\mathbf{x} | \mathbf{y})$ and $p(\mathbf{s} | \mathbf{y})$.

C. Example: Massive MIMO Channel Estimation under Hybrid Beamforming

Consider a narrowband massive MIMO system under a partially connected hybrid beamforming (PC-HBF) architecture, where the base station (BS) is equipped with N_r antennas and N_{RF} radio frequency (RF) chains with $N_{RF} < N_r$, as illustrated in Fig. 2. Each user is equipped with a single antenna. In the channel training stage, each user transmits an uplink pilot at different pilot symbols for the BS to estimate the channel. Without loss of generality, we focus on the channel estimation of one user, the received signal $\mathbf{y} \in \mathbb{C}^{N_{RF} \times 1}$ at the BS can be written as:

$$\mathbf{y} = \mathbf{F} \mathbf{h} u + \mathbf{w}, \quad (8)$$

where u is the pilot symbol, $\mathbf{h} \in \mathbb{C}^{N_r \times 1}$ is the channel vector of the user, $\mathbf{F} = \mathbf{F}_d \mathbf{F}_a \in \mathbb{C}^{N_{RF} \times N_r}$, $\mathbf{F}_a \in \mathbb{C}^{N_{RF} \times N_r}$ is the analog combining matrix, $\mathbf{F}_d \in \mathbb{C}^{N_{RF} \times N_{RF}}$ is the digital combining matrix, and $\mathbf{w} \sim \mathcal{CN}(0, \sigma^2 \mathbf{I}) \in \mathbb{C}^{N_{RF} \times 1}$ is the additive white Gaussian Noise (AWGN). Since the analog combining matrix is composed of a series of low-cost phase shifters, the non-zero elements of analog precoding matrix \mathbf{F}_a have unit modulus constraint. Moreover, in PC-HBF architecture, each RF chain is only connected to a subarray of the antennas, and thus \mathbf{F}_a is a block diagonal matrix with

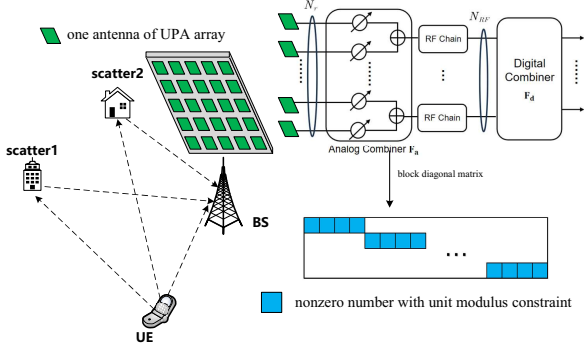


Figure 2: Illustration of channel estimation in PC-HBF massive MIMO system.

each block a row vector of $\frac{N_r}{N_{RF}}$ elements, as illustrated in Fig. 2. In the simulations, to ensure that \mathbf{F} satisfies the restricted isometry property (RIP) with high probability, the phases of the non-zero elements in \mathbf{F}_a are chosen to be i.i.d. with a uniform distribution over $[0, 2\pi]$ and the digital combining matrix \mathbf{F}_d is set as a random orthogonal matrix.

The channel vector \mathbf{h} can be represented as:

$$\mathbf{h} = \sum_{k=1}^K \alpha_k \mathbf{a}_R(\theta_k, \phi_k), \quad (9)$$

where α_k , θ_k and ϕ_k are the complex gain, azimuth angle of arrival (AoA), and elevation AoA of the k -th channel path, respectively, and $\mathbf{a}_R(\theta_k, \phi_k)$ is the array response vector that depends on the antenna array. In the simulations, we adopt a uniform planar array (UPA) with N_x antennas in the horizon direction and N_y antennas in the vertical direction. The grid-based method is adopted to obtain a sparse representation of massive MIMO channel for high-accuracy channel estimation. Similar to [19], we introduce a 2D dynamic angular-domain grid of $Q = N_1 \times N_2$ angle points, where the q -th grid point is denoted by (θ_q, ϕ_q) . Define $\boldsymbol{\theta} \triangleq [\theta_1, \dots, \theta_Q]^T$ and $\boldsymbol{\phi} \triangleq [\phi_1, \dots, \phi_Q]^T$ represent the dynamic grid vectors. The uniform angle grid is usually chosen as the initial value of the dynamic grid [15].

With the definition of the dynamic angular-domain grid, we can reformulate the received signal model in (8) as:

$$\mathbf{y} = \mathbf{u} \mathbf{F} \mathbf{A}(\boldsymbol{\theta}, \boldsymbol{\phi}) \mathbf{x} + \mathbf{w}, \quad (10)$$

with

$$\mathbf{A}(\boldsymbol{\theta}, \boldsymbol{\phi}) \triangleq [\mathbf{a}(\theta_1, \phi_1), \dots, \mathbf{a}(\theta_Q, \phi_Q)] \in \mathbb{C}^{N_r \times Q}, \quad (11)$$

$\mathbf{x} \in \mathbb{C}^{Q \times 1}$ is the angular-domain sparse channel vector, which has only $K \ll Q$ non-zero elements corresponding to K paths. Specifically, the q -th element of \mathbf{x} , denoted by x_q , is the complex gain of the channel path lying around the q -th angle grid point.

The angular-domain sparse channel vector \mathbf{x} exhibits a 2D clustered sparsity, i.e., if we arrange \mathbf{x} into an $N_1 \times N_2$ matrix, the non-zero elements of \mathbf{x} will concentrate on a few non-zero 2D clusters [20]. We design a 2D Markov model [21] to capture the 2D clustered sparsity in the angular

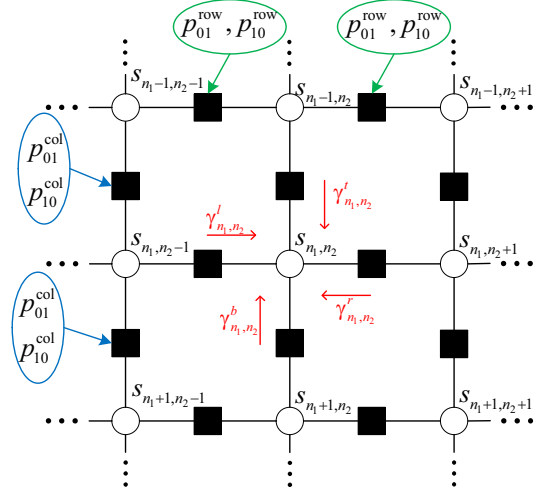


Figure 3: The factor graph of the 2D Markov model.

domain. For convenience, we use s_{n_1, n_2} to represent the $((n_2 - 1)N_1 + n_1)$ -th element of \mathbf{s} . The support vector is modeled as

$$p(\mathbf{s}) = p(s_{1,1}) \prod_{n_1=1}^{N_1} \prod_{n_2=2}^{N_2} p(s_{n_1, n_2} | s_{n_1, n_2-1}) \times \prod_{n_1=2}^{N_1} \prod_{n_2=1}^{N_2} p(s_{n_1, n_2} | s_{n_1-1, n_2}), \quad (12)$$

with the transition probability given by

$$p_{01}^{\text{row}} = p(s_{n_1, n_2} = 1 | s_{n_1, n_2-1} = 0), \quad (13a)$$

$$p_{10}^{\text{row}} = p(s_{n_1, n_2} = 0 | s_{n_1, n_2-1} = 1), \quad (13b)$$

$$p_{01}^{\text{col}} = p(s_{n_1, n_2} = 1 | s_{n_1-1, n_2} = 0), \quad (13c)$$

$$p_{10}^{\text{col}} = p(s_{n_1, n_2} = 0 | s_{n_1-1, n_2} = 1). \quad (13d)$$

The work in [21] verified that a set of $\{p_{01}^{\text{row}}, p_{10}^{\text{row}}, p_{01}^{\text{col}}, p_{10}^{\text{col}}\}$ can be found to satisfy the steady-state condition of the 2D Markov model, i.e., $p(s_{1,1} = 1) = \lambda$, where λ denotes the sparsity level of \mathbf{s} . As such, the initial distribution $p(s_{1,1})$ is set to be the steady-state distribution, $p(s_{1,1} = 1) = \lambda$.

We show the factor graph of the 2D Markov model in Fig. 3. The value of $\{p_{01}^{\text{row}}, p_{10}^{\text{row}}, p_{01}^{\text{col}}, p_{10}^{\text{col}}\}$ will affect the structure of clusters. Specifically, smaller p_{10}^{row} and p_{10}^{col} imply a larger average cluster size, and smaller p_{01}^{row} and p_{01}^{col} imply a larger average gap between two adjacent clusters.

III. THE PROPOSED ALTERNATING ESTIMATION FRAMEWORK

It is very challenging to calculate the exact posterior $p(\mathbf{x} | \mathbf{y})$ and $p(\mathbf{s} | \mathbf{y})$ because the factor graph of the associated joint probability model has loops. In this section, we shall propose an alternating estimation (AE) framework to approximately calculate the marginal posteriors $p(\mathbf{x} | \mathbf{y})$ and $p(s_n | \mathbf{y}), \forall n$, and finds an approximate solution for MLE problem $\arg\max_{\boldsymbol{\theta}} \ln p(\boldsymbol{\theta} | \mathbf{y})$. The proposed AE framework is shown in the simulations to achieve a good performance.

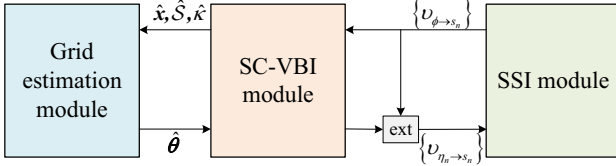


Figure 4: The basic modules of the alternating estimation framework.

As illustrated in Fig. 4, the AE framework iterates among the following three modules until convergence.

- **SC-VBI Module:** For fixed ML estimator $\hat{\theta}$ of θ from the grid estimation (GE) module and extrinsic message $v_{\phi \rightarrow s_n}(s_n), \forall n$ from the structured sparse inference (SSI) module (which can be viewed as prior information for SC-VBI), the SC-VBI module computes a Bayesian estimation of the collection of parameters $\mathbf{v} = \{\mathbf{x}, \boldsymbol{\rho}, \mathbf{s}, \kappa\}$, from which it outputs MMSE estimators $\hat{\mathbf{x}}$ and $\hat{\kappa}$ of \mathbf{x} and κ , the estimated support $\hat{\mathcal{S}}$, and extrinsic message $v_{\eta_n \rightarrow s_n}(s_n), \forall n$.
- **Grid Estimation Module:** For fixed $\hat{\mathbf{x}}, \hat{\mathcal{S}}$, and $\hat{\kappa}$ output from the SC-VBI module, the grid estimation module refines the dynamic grid by directly maximizing the likelihood function based on the gradient ascent method with backtracking line search.
- **Structured Sparse Inference Module:** For fixed extrinsic message $v_{\eta_n \rightarrow s_n}(s_n), \forall n$ from the SC-VBI module (which can be viewed as prior information for SSI), the SSI module performs sum-product message passing over the structured sparse prior to exploit the specific sparse structures in practical applications.

In the following, we shall outline the GE and SSI modules, and explain the calculation of the extrinsic messages between the SC-VBI and SSI. The details of the proposed SC-VBI module will be presented in Section IV.

A. The Grid Estimation Module

To reduce the complexity, we only retain the sparse signals and grid parameters indexed by the estimated support $\hat{\mathcal{S}}$ and remove all other signals and grid parameters. In this case, for fixed $\hat{\mathbf{x}}, \hat{\mathcal{S}}$ and $\hat{\kappa}$ output from the SC-VBI module, the logarithmic likelihood function of θ is expressed as

$$\mathcal{L}(\theta_{\hat{\mathcal{S}}}) \triangleq -\hat{\kappa} \|\mathbf{y} - \mathbf{A}_{\hat{\mathcal{S}}}(\theta_{\hat{\mathcal{S}}}) \hat{\mathbf{x}}_{\hat{\mathcal{S}}}\|^2 + C, \quad (14)$$

where C is a constant, and $\mathbf{A}_{\hat{\mathcal{S}}} \in \mathbb{C}^{M \times |\hat{\mathcal{S}}|}$ is a submatrix of \mathbf{A} with the column indices lying in $\hat{\mathcal{S}}$. It is difficult to find the optimal $\theta_{\hat{\mathcal{S}}}$ that maximizes $\mathcal{L}(\theta_{\hat{\mathcal{S}}})$ since $\mathcal{L}(\theta_{\hat{\mathcal{S}}})$ is non-concave w.r.t. $\theta_{\hat{\mathcal{S}}}$. In this case, a gradient ascent approach is usually employed to update $\theta_{\hat{\mathcal{S}}}$. Specifically, in the i -th iteration, the grid parameters are updated as

$$\theta_{\hat{\mathcal{S}}}^{(i)} = \theta_{\hat{\mathcal{S}}}^{(i-1)} + \epsilon_{\theta}^{(i)} \nabla_{\theta_{\hat{\mathcal{S}}}} \mathcal{L}(\theta_{\hat{\mathcal{S}}}) |_{\theta_{\hat{\mathcal{S}}} = \theta_{\hat{\mathcal{S}}}^{(i-1)}}, \quad (15)$$

where $\epsilon_{\theta}^{(i)}$ is the step size determined by the Armijo rule. The other grid parameters which are not indexed by $\hat{\mathcal{S}}$ are set to equal to the previous iteration. We can apply the above

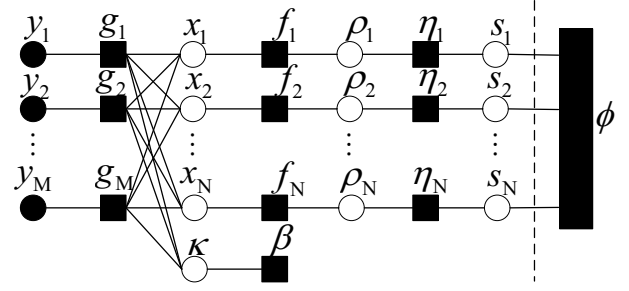


Figure 5: Factor graph of the joint distribution $p(\mathbf{v}, \mathbf{y})$.

Table I: Factors, Distributions and Functional forms in Fig. 5. $\mathbf{A}_m(\theta)$ denotes the m -th row of $\mathbf{A}(\theta)$.

Factor	Distribution	Functional form
g_m	$p(y_m \mathbf{x}, \kappa)$	$\mathcal{CN}(y_m; \mathbf{A}_m(\theta) \mathbf{x}, \kappa^{-1})$
f_n	$p(x_n \rho_n)$	$\mathcal{CN}(x_n; 0, \rho_n^{-1})$
η_n	$p(\rho_n s_n)$	$\begin{cases} \Gamma(\rho_n; a_n, b_n), & s_n = 1 \\ \Gamma(\rho_n; \bar{a}_n, \bar{b}_n), & s_n = 0 \end{cases}$
ϕ	$p(\mathbf{s})$	e.g., (12)
β	$p(\kappa)$	$\Gamma(\kappa; c, d)$

gradient update for $B_{\theta} \geq 1$ times, where B_{θ} is chosen to achieve a good trade-off between the per iteration complexity and convergence speed.

B. Calculation of the Extrinsic Messages between SC-VBI and SSI

For fixed grid parameters $\hat{\theta}$, the factor graph of the joint distribution $p(\mathbf{v}, \mathbf{y})$ is shown in Fig. 5, while the associated factor nodes are listed in Table I. Due to the existence of many loops in this factor graph, we cannot directly apply the message passing method to calculate the posterior. In this case, the turbo approach is often used to decouple the observation model and structured sparse prior model such that the Bayesian inference in each model is more tractable [6].

Specifically, we first partition the factor graph in Fig. 5 along the dash line into two decoupled subgraphs, denoted by \mathcal{G}_A and \mathcal{G}_B , as shown in Fig. 6. To be more specific, \mathcal{G}_A describes the structure of the observation model with an independent sparse prior, while \mathcal{G}_B describes the more complicated sparse structure of the support vector \mathbf{s} . Then we design SC-VBI and SSI modules to perform Bayesian inference over the two subgraphs. For \mathcal{G}_A , the SC-VBI module is adopted to compute each variational distribution approximately. For \mathcal{G}_B , sum-product message passing is adopted to compute the marginal posterior of \mathbf{s} . The two modules exchange extrinsic messages until converge. And the output messages of one module form the priors for another module. Specifically, the extrinsic messages from SC-VBI to SSI are denoted by $\{v_{\eta_n \rightarrow s_n}\}$, while the extrinsic messages from SSI to SC-VBI are denoted by $\{v_{\phi \rightarrow s_n}\}$. Formally, we define two turbo-iteration factor nodes:

$$\begin{aligned} \phi_{A,n}(s_n) &\triangleq v_{\phi \rightarrow s_n}(s_n), n = 1, \dots, N, \\ \phi_{B,n}(s_n) &\triangleq v_{\eta_n \rightarrow s_n}(s_n), n = 1, \dots, N, \end{aligned} \quad (16)$$

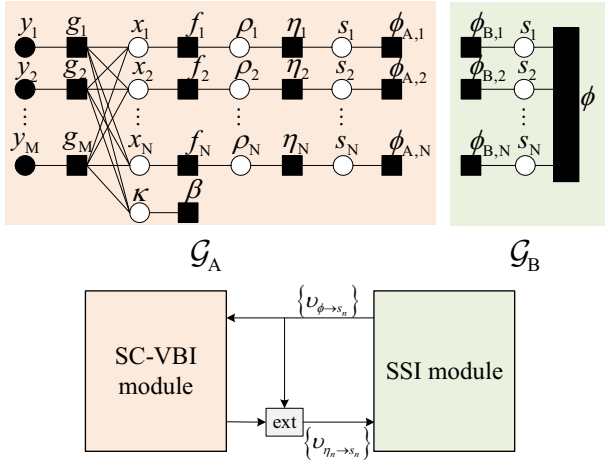


Figure 6: The turbo approach yields a decoupled factor graph. The extrinsic messages flow between the SC-VBI module and the SSI module.

where $\phi_{A,n}(s_n)$ can be viewed as the prior information for the SC-VBI Module. And for each turbo iteration, the extrinsic message $v_{\eta_n \rightarrow s_n}(s_n)$ from SC-VBI to SSI can be computed by subtracting the prior information $\phi_{A,n}(s_n)$ from posterior information,

$$v_{\eta_n \rightarrow s_n}(s_n) \propto q(s_n) / \phi_{A,n}(s_n), \quad (17)$$

where $q(s_n)$ is the approximate posterior distribution obtained by the SC-VBI as in (30). On the other hand, the extrinsic message $v_{\phi \rightarrow s_n}(s_n)$ from SSI to SC-VBI can be directly computed by message passing over \mathcal{G}_B .

C. The Structured Sparse Inference Module

The sum-product message passing algorithm for the SSI module depends on the specific sparse prior model in practical applications. In this subsection, we use the massive MIMO channel estimation under the 2D Markov prior model described in Subsection II-C as a concrete example to illustrate how the SSI Module performs message passing.

The factor graph of the MRF model in (12) is given in Fig. 3. As discussed in subsection II-C, we use n_1, n_2 to index the support vector \mathbf{s} in this subsection. To simplify the notation, we use π_{n_1, n_2}^{in} to abbreviate $\phi_{B,n}(s_n = 1)$ with $n = (n_2 - 1)N_1 + n_1$. In the following, we obey the sum-product rule to derive messages over the factor graph [22].

For s_{n_1, n_2} , the input messages from the left, right, top, and bottom factor nodes, denoted by $v_{n_1, n_2}^l, v_{n_1, n_2}^r, v_{n_1, n_2}^t,$ and v_{n_1, n_2}^b , respectively, follow Bernoulli distributions, which can be calculated as

$$v_{n_1, n_2}^d = \gamma_{n_1, n_2}^d \delta(s_{n_1, n_2} - 1) + (1 - \gamma_{n_1, n_2}^d) \delta(s_{n_1, n_2}),$$

for $d \in \{l, r, t, b\}$, with $\gamma_{n_1, n_2}^d, d \in \{l, r, t, b\}$ given at the top of the next page.

Then the output message for s_{n_1, n_2} (i.e., the extrinsic message from the SSI module to the SC-VBI module) can

be calculated as

$$\begin{aligned} v_{\phi \rightarrow s_{n_1, n_2}} &\propto \prod_{d \in \{l, r, t, b\}} v_{n_1, n_2}^d \\ &\propto \pi_{n_1, n_2}^{out} \delta(s_{n_1, n_2} - 1) + (1 - \pi_{n_1, n_2}^{out}) \delta(s_{n_1, n_2}) \end{aligned} \quad (19)$$

where

$$\pi_n^{out} = \frac{\prod_{d \in \{l, r, t, b\}} \gamma_{n_1, n_2}^d}{\prod_{d \in \{l, r, t, b\}} \gamma_{n_1, n_2}^d + \prod_{d \in \{l, r, t, b\}} (1 - \gamma_{n_1, n_2}^d)}.$$

IV. SUBSPACE CONSTRAINED VARIATIONAL BAYESIAN INFERENCE

A. VBI Problem Formulation for the SC-VBI Module

Based on the observation \mathbf{y} and extrinsic message $\phi_{A,n}(s_n) \triangleq v_{\phi \rightarrow s_n}(s_n), \forall n$ from the SSI module, the SC-VBI module adopts VBI [18] to calculate the approximate marginal posteriors $q(\mathbf{v})$ for fixed grid parameters $\hat{\boldsymbol{\theta}}$. To be more specific, the turbo-iteration factor nodes $\phi_{A,n}(s_n), \forall n$ incorporate the prior information from the SSI module. Therefore, the following prior distribution is assumed when performing the VBI in the SC-VBI module:

$$\begin{aligned} \hat{p}(\mathbf{x}, \boldsymbol{\rho}, \mathbf{s}) &= \hat{p}(\mathbf{s}) p(\boldsymbol{\rho} | \mathbf{s}) p(\mathbf{x} | \boldsymbol{\rho}), \\ \hat{p}(\mathbf{s}) &= \prod_{n=1}^N \phi_{A,n}(s_n). \end{aligned} \quad (20)$$

Since the grid parameter is fixed in SC-VBI, we omit the grid parameter $\hat{\boldsymbol{\theta}}$ and use \mathbf{A} as a simplified notation for $\mathbf{A}(\hat{\boldsymbol{\theta}})$.

For convenience, we use \mathbf{v}^k to denote an individual variable in $\mathbf{v} \triangleq \{\mathbf{x}, \boldsymbol{\rho}, \mathbf{s}, \boldsymbol{\kappa}\}$. Let $\mathcal{H} = \{k | \forall \mathbf{v}^k \in \mathbf{v}\}$ and denote $\hat{p}(\mathbf{v} | \mathbf{y})$ as the posterior distribution of \mathbf{v} with the prior $\hat{p}(\mathbf{x}, \boldsymbol{\rho}, \mathbf{s})$ in (20). Based on the VBI method, the approximate marginal posterior could be calculated by minimizing the KLD between $\hat{p}(\mathbf{v} | \mathbf{y})$ and $q(\mathbf{v})$, subject to a factorized form constraint as [18]

$$\mathcal{A}_{VBI}: \quad q^*(\mathbf{v}) = \arg \min_{q(\mathbf{v})} \int q(\mathbf{v}) \ln \frac{q(\mathbf{v})}{\hat{p}(\mathbf{v} | \mathbf{y})} d\mathbf{v}, \quad (21)$$

$$\text{s.t.} \quad q(\mathbf{v}) = \prod_{k \in \mathcal{H}} q(\mathbf{v}^k), \quad \int q(\mathbf{v}^k) d\mathbf{v}^k = 1, \quad (22)$$

$$q(\mathbf{x}) = \mathcal{CN}(\mathbf{x}; \boldsymbol{\mu}, \text{diag}(\boldsymbol{\sigma}^2)). \quad (23)$$

Note that we add an additional constraint that $q(\mathbf{x})$ is a Gaussian distribution with mean $\boldsymbol{\mu}$ and diagonal covariance matrix $\text{diag}(\boldsymbol{\sigma}^2)$, where both the mean $\boldsymbol{\mu}$ and variance vector $\boldsymbol{\sigma}^2 = [\sigma_1^2, \dots, \sigma_N^2]^T$ are optimization variables. This additional constraint is imposed to avoid the high dimensional matrix inverse for calculating the posterior covariance matrix. On the other hand, the high dimensional matrix inverse for calculating the posterior mean will be avoided using the subspace constrained method.

Solving \mathcal{A}_{VBI} yields a good approximation of the true posterior $\hat{p}(\mathbf{v} | \mathbf{y})$ [18]. Since Problem \mathcal{A}_{VBI} is non-convex, we aim at finding a stationary solution (denoted by $q^*(\mathbf{v})$) of \mathcal{A}_{VBI} , as defined below.

$$\gamma_{n_1, n_2}^l = \frac{p_{11}^{\text{row}} \pi_{n_1, n_2-1}^{\text{in}} \prod_{d \in \{l, t, b\}} \gamma_{n_1, n_2-1}^d + p_{01}^{\text{row}} (1 - \pi_{n_1, n_2-1}^{\text{in}}) \prod_{d \in \{l, t, b\}} (1 - \gamma_{n_1, n_2-1}^d)}{\pi_{n_1, n_2-1}^{\text{in}} \prod_{d \in \{l, t, b\}} \gamma_{n_1, n_2-1}^d + (1 - \pi_{n_1, n_2-1}^{\text{in}}) \prod_{d \in \{l, t, b\}} (1 - \gamma_{n_1, n_2-1}^d)}, \quad (18a)$$

$$\gamma_{n_1, n_2}^r = \frac{p_{11}^{\text{row}} \pi_{n_1, n_2+1}^{\text{in}} \prod_{d \in \{r, t, b\}} \gamma_{n_1, n_2+1}^d + p_{10}^{\text{row}} (1 - \pi_{n_1, n_2+1}^{\text{in}}) \prod_{d \in \{r, t, b\}} (1 - \gamma_{n_1, n_2+1}^d)}{(p_{11}^{\text{row}} + p_{01}^{\text{row}}) \pi_{n_1, n_2+1}^{\text{in}} \prod_{d \in \{r, t, b\}} \gamma_{n_1, n_2+1}^d + (p_{00}^{\text{row}} + p_{10}^{\text{row}}) (1 - \pi_{n_1, n_2+1}^{\text{in}}) \prod_{d \in \{r, t, b\}} (1 - \gamma_{n_1, n_2+1}^d)}, \quad (18b)$$

$$\gamma_{n_1, n_2}^t = \frac{p_{11}^{\text{col}} \pi_{n_1-1, n_2}^{\text{in}} \prod_{d \in \{l, r, t\}} \gamma_{n_1-1, n_2}^d + p_{01}^{\text{col}} (1 - \pi_{n_1-1, n_2}^{\text{in}}) \prod_{d \in \{l, r, t\}} (1 - \gamma_{n_1-1, n_2}^d)}{\pi_{n_1-1, n_2}^{\text{in}} \prod_{d \in \{l, r, t\}} \gamma_{n_1-1, n_2}^d + (1 - \pi_{n_1-1, n_2}^{\text{in}}) \prod_{d \in \{l, r, t\}} (1 - \gamma_{n_1-1, n_2}^d)}, \quad (18c)$$

$$\gamma_{n_1, n_2}^b = \frac{p_{11}^{\text{col}} \pi_{n_1+1, n_2}^{\text{in}} \prod_{d \in \{l, r, b\}} \gamma_{n_1+1, n_2}^d + p_{10}^{\text{col}} (1 - \pi_{n_1+1, n_2}^{\text{in}}) \prod_{d \in \{l, r, b\}} (1 - \gamma_{n_1+1, n_2}^d)}{(p_{11}^{\text{col}} + p_{01}^{\text{col}}) \pi_{n_1+1, n_2}^{\text{in}} \prod_{d \in \{l, r, b\}} \gamma_{n_1+1, n_2}^d + (p_{00}^{\text{col}} + p_{10}^{\text{col}}) (1 - \pi_{n_1+1, n_2}^{\text{in}}) \prod_{d \in \{l, r, b\}} (1 - \gamma_{n_1+1, n_2}^d)}, \quad (18d)$$

Definition 1 (Stationary Solution). $q^*(\mathbf{v}) = \prod_{k \in \mathcal{H}} q^*(\mathbf{v}^k)$ is called a stationary solution of Problem \mathcal{A}_{VBI} if it satisfies all the constraints in \mathcal{A}_{VBI} and $\forall k \in \mathcal{H}$,

$$q^*(\mathbf{v}^k) = \arg \min_{q(\mathbf{v}^k)} \int \prod_{l \neq k} q^*(\mathbf{v}^l) q(\mathbf{v}^k) \ln \frac{\prod_{l \neq k} q^*(\mathbf{v}^l) q(\mathbf{v}^k)}{\hat{p}(\mathbf{v} | \mathbf{y})}.$$

In particular, when $\mathbf{v}^k = \mathbf{x}$, the above minimization is over the optimization variables $\boldsymbol{\mu}, \boldsymbol{\sigma}^2$ in $q(\mathbf{x}) = \mathcal{CN}(\mathbf{x}; \boldsymbol{\mu}, \text{diag}(\boldsymbol{\sigma}^2))$.

By finding a stationary solution $q^*(\mathbf{v})$ of \mathcal{A}_{VBI} , we could obtain the approximate posterior $q^*(\mathbf{v}^k) \approx p(\mathbf{v}^k | \mathbf{y})$.

When there is no additional constraint of $q(\mathbf{x}) = \mathcal{CN}(\mathbf{x}; \boldsymbol{\mu}, \text{diag}(\boldsymbol{\sigma}^2))$, the problem of finding a stationary solution $q^*(\mathbf{v})$ of \mathcal{A}_{VBI} has been addressed in [9] using a sparse VBI algorithm, where the update of $q(\mathbf{x})$ involves a high-dimensional matrix inverse. In the following, we shall first derive a VBI algorithm for \mathcal{A}_{VBI} with constraint $q(\mathbf{x}) = \mathcal{CN}(\mathbf{x}; \boldsymbol{\mu}, \text{diag}(\boldsymbol{\sigma}^2))$, which is called independence constrained VBI (IC-VBI) since the approximate posterior $q(\mathbf{x})$ are product of independently Gaussian distributions of x_n . Then we modify the update equation of the posterior mean in $q(\mathbf{x})$ to obtain a low-complexity SC-VBI algorithm.

B. Derivation of the IC-VBI Algorithm for \mathcal{A}_{VBI}

The IC-VBI algorithm finds a stationary solution of \mathcal{A}_{VBI} via alternately optimizing each individual density $q(\mathbf{v}^k)$, $k \in \mathcal{H}$. Specifically, for given $q(\mathbf{v}^l)$, $\forall l \neq k$ and $\mathbf{v}^k \neq \mathbf{x}$, the optimal $q(\mathbf{v}^k)$ that minimizes the KLD in \mathcal{A}_{VBI} is given by [18]

$$q(\mathbf{v}^k) \propto \exp\left(\langle \ln \hat{p}(\mathbf{v}, \mathbf{y}) \rangle_{\prod_{l \neq k} q(\mathbf{v}^l)}\right), \quad (24)$$

where $\langle f(\mathbf{x}) \rangle_{q(\mathbf{x})} = \int f(\mathbf{x}) q(\mathbf{x}) d\mathbf{x}$ and $\hat{p}(\mathbf{v}, \mathbf{y})$ is the joint PDF with prior $\hat{p}(\mathbf{x}, \boldsymbol{\rho}, \mathbf{s})$, i.e.,

$$\hat{p}(\mathbf{v}, \mathbf{y}) = p(\mathbf{y} | \mathbf{x}, \boldsymbol{\kappa}) \hat{p}(\mathbf{x}, \boldsymbol{\rho}, \mathbf{s}) p(\boldsymbol{\kappa}), \quad (25)$$

where $p(\mathbf{y} | \mathbf{x}, \boldsymbol{\kappa}) = \mathcal{CN}(\mathbf{y}; \mathbf{A}\mathbf{x}, \boldsymbol{\kappa}^{-1} \mathbf{I}_M)$ is the likelihood function. However, when $\mathbf{v}^k = \mathbf{x}$, the optimal $q(\mathbf{x})$ is no longer given by (24) due to the independence constraint, and it is characterized by the following lemma. Note that the expectation $\langle f(\mathbf{v}^k) \rangle_{q(\mathbf{v}^k)}$ w.r.t. its own approximate posterior will be simplified as $\langle f(\mathbf{v}^k) \rangle$.

Lemma 2. For given $q(\boldsymbol{\rho}), q(\mathbf{s}), q(\boldsymbol{\kappa})$, \mathcal{A}_{VBI} is equivalent to the following optimization problem

$$\min_{\mathbf{u}, \boldsymbol{\sigma}^2} \mathbf{u}^H \mathbf{W} \mathbf{u} - 2\Re\{\mathbf{u}^H \mathbf{b}\} + \sum_{n=1}^N (W_n \sigma_n^2 - \ln \sigma_n^2), \quad (26)$$

where $\mathbf{W} = \text{diag}(\langle \boldsymbol{\rho} \rangle) + \langle \boldsymbol{\kappa} \rangle \mathbf{A}^H \mathbf{A}$ and $\mathbf{b} = \langle \boldsymbol{\kappa} \rangle \mathbf{A}^H \mathbf{y}$, W_n is the n -th diagonal element of \mathbf{W} . In other words, for given $q(\boldsymbol{\rho}), q(\mathbf{s}), q(\boldsymbol{\kappa})$, the optimal posterior mean $\boldsymbol{\mu}$ and variance vector $\boldsymbol{\sigma}^2$ in $q(\mathbf{x})$ that minimizes the KLD subject to $q(\mathbf{x}) = \mathcal{CN}(\mathbf{x}; \boldsymbol{\mu}, \text{diag}(\boldsymbol{\sigma}^2))$ are given by the

$$\begin{aligned} \boldsymbol{\mu} &= \underset{\mathbf{u}}{\text{argmin}} \varphi(\mathbf{u}) \triangleq \mathbf{u}^H \mathbf{W} \mathbf{u} - 2\Re\{\mathbf{u}^H \mathbf{b}\}, \\ \boldsymbol{\sigma}^2 &= [W_1^{-1}, W_2^{-1}, \dots, W_N^{-1}]. \end{aligned}$$

Please refer to Appendix A for the detailed proof. Based on (24) and Lemma 2, the update equations of all variables are given in the subsequent subsections.

1) *Update Equation for $q(\mathbf{x})$* : From Lemma 2, $q(\mathbf{x})$ can be derived as

$$q(\mathbf{x}) = \mathcal{CN}(\mathbf{x}; \boldsymbol{\mu}, \boldsymbol{\sigma}^2), \quad (27)$$

where $\boldsymbol{\mu} = \mathbf{W}^{-1} \mathbf{b}$ and $\boldsymbol{\sigma}^2 = [W_1^{-1}, W_2^{-1}, \dots, W_N^{-1}]$.

2) *Update Equation for $q(\boldsymbol{\rho})$* : $q(\boldsymbol{\rho})$ can be derived as

$$q(\boldsymbol{\rho}) = \prod_{n=1}^N \Gamma(\rho_n; \tilde{a}_n, \tilde{b}_n), \quad (28)$$

where the approximate posterior parameters are given by:

$$\begin{aligned} \tilde{a}_n &= \langle s_n \rangle a_n + \langle 1 - s_n \rangle \bar{a}_n + 1, \\ \tilde{b}_n &= \langle s_n \rangle b_n + \langle 1 - s_n \rangle \bar{b}_n + \langle |x_n|^2 \rangle. \end{aligned} \quad (29)$$

3) *Update Equation for $q(\mathbf{s})$* : $q(\mathbf{s})$ can be derived as

$$q(\mathbf{s}) = \prod_{n=1}^N (\tilde{\lambda}_n)^{s_n} (1 - \tilde{\lambda}_n)^{1-s_n}, \quad (30)$$

where $\tilde{\lambda}_n$ is given by

$$\tilde{\lambda}_n = \frac{\lambda_n C_n}{\lambda_n C_n + (1 - \lambda_n) \bar{C}_n}, \quad (31)$$

with $\lambda_n = \phi_{A,n}(s_n = 1)$, $C_n = \frac{b_n^{a_n}}{\Gamma(a_n)} \exp((a_n - 1) \langle \ln \rho_n \rangle - b_n \langle \rho_n \rangle)$, and $\bar{C}_n =$

$\frac{\bar{b}_n^{\bar{a}_n}}{\Gamma(\bar{a}_n)} \exp((\bar{a}_n - 1) \langle \ln \rho_n \rangle - \bar{b}_n \langle \rho_n \rangle)$. Here, $\Gamma(\cdot)$ denotes the gamma function.

4) *Update Equation for $q(\kappa)$* : The posterior distribution $q(\kappa)$ is given by

$$q(\kappa) = \Gamma(\kappa; \tilde{c}, \tilde{d}), \quad (32)$$

where the parameters \tilde{c} and \tilde{d} are given by

$$\begin{aligned} \tilde{c} &= c + M, \\ \tilde{d} &= d + \left\langle \|\mathbf{y} - \mathbf{A}\mathbf{x}\|^2 \right\rangle_{q(\mathbf{x})}. \end{aligned} \quad (33)$$

The expectations used in the above update equations are summarized as follows:

$$\begin{aligned} \langle \rho_n \rangle &= \frac{\tilde{a}_n}{\tilde{b}_n} & \langle \boldsymbol{\rho} \rangle &= [\langle \rho_1 \rangle, \dots, \langle \rho_N \rangle]^T & \langle s_n \rangle &= \tilde{\lambda}_n \\ \langle \gamma \rangle &= \frac{\tilde{c}}{\tilde{d}} & \langle x_n^2 \rangle &= |\mu_n|^2 + \sigma_n^2 & \langle \ln \rho_n \rangle &= \psi(\tilde{a}_n) - \ln \tilde{b}_n, \end{aligned}$$

where μ_n is the n -th element of $\boldsymbol{\mu}$ and $\psi(\cdot) \triangleq d \ln(\Gamma(\cdot))$ denotes the logarithmic derivative of the gamma function.

C. The Proposed SC-VBI Algorithm

1) *The Basic Version*: The complexity of the IC-VBI algorithm in the above is dominated by the high-dimensional matrix inverse operation $\boldsymbol{\mu} = \mathbf{W}^{-1}\mathbf{b}$ in the update of $q(\mathbf{x})$. Recall that posterior mean $\boldsymbol{\mu}$ is the optimal solution of the following quadratic programming problem:

$$\min_{\mathbf{u}} \varphi(\mathbf{u}) \triangleq \mathbf{u}^H \mathbf{W} \mathbf{u} - 2\Re\{\mathbf{u}^H \mathbf{b}\}. \quad (34)$$

Let $\hat{\mathcal{S}}$ denote the estimated support of \mathbf{x} obtained in the previous iteration, as will be detailed soon. If $\hat{\mathcal{S}} = \mathcal{S}$, then the LMMSE of $\mathbf{x}_{\hat{\mathcal{S}}}$, given by

$$\boldsymbol{\mu}_{\hat{\mathcal{S}}}^0 = \langle \kappa \rangle \mathbf{W}_{\hat{\mathcal{S}}}^{-1} \mathbf{A}_{\hat{\mathcal{S}}}^H \mathbf{y}, \quad (35)$$

should be a very good estimation for the non-zero elements in \mathbf{x} , where $\mathbf{W}_{\hat{\mathcal{S}}} \in \mathbb{C}^{|\hat{\mathcal{S}}| \times |\hat{\mathcal{S}}|}$ is a submatrix of \mathbf{W} with the column/row indices lying in $\hat{\mathcal{S}}$.

In other words, if we define a vector $\boldsymbol{\mu}^0$ such that $\boldsymbol{\mu}_{\hat{\mathcal{S}}}^0 = \langle \kappa \rangle \mathbf{W}_{\hat{\mathcal{S}}}^{-1} \mathbf{A}_{\hat{\mathcal{S}}}^H \mathbf{y}$ and $\boldsymbol{\mu}_n^0 = \mathbf{0}, \forall n \notin \hat{\mathcal{S}}$, then $\boldsymbol{\mu}^0$ is expected to provide a good initial solution for Problem ((34)). Then starting from this initial point, we apply the gradient update for $B_x \geq 1$ times. Specifically, in the i -th iteration, the posterior mean is updated as

$$\boldsymbol{\mu}^{(i)} = \boldsymbol{\mu}^{(i-1)} - \epsilon_x^{(i)} \nabla_{\mathbf{u}} \varphi(\mathbf{u}) \big|_{\mathbf{u}=\boldsymbol{\mu}^{(i-1)}}, \quad (36)$$

where $\epsilon_x^{(i)}$ is the step size determined by the Armijo rule,

$$\nabla_{\mathbf{u}} \varphi(\mathbf{u} = \boldsymbol{\mu}^{(i-1)}) = \mathbf{W} \boldsymbol{\mu}^{(i-1)} - \langle \kappa \rangle \mathbf{A}^H \mathbf{y}, \quad (37)$$

and B_x is chosen to achieve a good tradeoff between the per iteration complexity and convergence speed.

2) *Support Estimation*: Once we obtain the estimated posterior mean $\boldsymbol{\mu}$, we can obtain an estimated support $\hat{\mathcal{S}}$ for the next iteration by finding the elements in $\boldsymbol{\mu}$ with sufficiently large energy. Specifically, we set a small threshold $\varepsilon > 0$ and

compare each element of $\boldsymbol{\mu}$ with the threshold to obtain the estimated support as

$$\hat{\mathcal{S}} \triangleq \left\{ n \mid |\mu_n|^2 > \varepsilon \right\}, \quad (38)$$

where the threshold ε is chosen according to the noise power $1/\langle \kappa \rangle$. A good choice for ε is 2 to 3 times the noise power $1/\langle \kappa \rangle$. Another option is to choose the largest $|\hat{\mathcal{S}}|$ elements that contain most of the total energy of $\boldsymbol{\mu}$, e.g., contain 95% of the total energy.

In the first iteration, we can simply set $\hat{\mathcal{S}}$ according to the available prior information in practice (e.g., in massive MIMO channel estimation, we may obtain a rough estimate of the support according to the previously estimated channels) or a simple baseline algorithm (e.g., using OMP).

3) *Robust Design Against Support Estimation Error*: To improve the robustness of the algorithm against the support estimation error, we choose the best initial point from the following two choices: 1) $\boldsymbol{\mu}_{\hat{\mathcal{S}}}^0$ obtained by the subspace constrained matrix inverse as in (35); 2) the posterior mean from the previous iteration, depending on which choice gives a lower value of the objective function $\varphi(\boldsymbol{\mu}^0)$. The motivations behind those two choices are as follows. In the first few iterations, $\boldsymbol{\mu}_{\hat{\mathcal{S}}}^0$ is expected to be a good choice because the subspace constrained matrix inverse can be used to accelerate the initial convergence speed, compared to the MM-based methods in [13]–[15] which completely avoid any matrix inverse. As the iterations go on, the posterior mean from the previous iteration becomes more and more accurate and it may also become a good initial point for the gradient update in (36).

D. Convergence Analysis

The convergence analysis for IC-VBI is straightforward. Each step of IC-VBI monotonically decreases the KLD until convergence to a stationary point. However, the convergence analysis for SC-VBI is quite challenging. First, the support estimation error may cause the algorithm fluctuate. Fortunately, this problem can be addressed by the robust design mentioned above, which ensures that the KLD is at least non-increasing. Second, when updating $q(\mathbf{x})$, we do not solve the subproblem in (26) exactly but only apply a few gradient update for the posterior mean $\boldsymbol{\mu}$ with the initial point give by the robust design described above. In the following, we show that the proposed SC-VBI still converges to a stationary point of \mathcal{A}_{VBI} , despite the above approximations and inexact update.

Theorem 3 (Convergence of SC-VBI). *With the robust design in Subsection (IV-C3), the SC-VBI algorithm monotonically decrease the KLD objective in \mathcal{A}_{VBI} , and every limiting point $q^*(\mathbf{v}) = \prod_{k \in \mathcal{H}} q^*(\mathbf{v}^k)$ generated by the SC-VBI is a stationary solution of Problem \mathcal{A}_{VBI} .*

Please refer to Appendix B for the detailed proof. The overall AE framework with SC-VBI as the key module (AE-SC-VBI) is summarized in Algorithm 1. In the first iteration, we may run the SC-VBI module for multiple times to obtain a better initial estimation, and in the rest iterations, we only need to run the SC-VBI module once per iteration to make the overall convergence speed faster.

Algorithm 1 AE-SC-VBI algorithm

Input: \mathbf{y} , $\mathbf{A}(\boldsymbol{\theta})$, maximum iteration number I .**Output:** $\hat{\mathbf{x}}$ and $\hat{\boldsymbol{\theta}}$.

- 1: **for** $k = 1, \dots, I$ **do**
 - 2: **SC-VBI Module:**
 - 3: Initialize the distribution functions $q(s)$, $q(\boldsymbol{\rho})$ and $q(\kappa)$.
 - 4: Update $q^k(\mathbf{x})$ using (27), where the posterior mean $\boldsymbol{\mu}$ is obtained by performing the gradient update (36) for B_x times with initial point in (35).
 - 5: Update $q^k(\boldsymbol{\rho})$ using (28).
 - 6: Update $q^k(s)$ using (30).
 - 7: Update $q^k(\kappa)$ using (32).
 - 8: Obtain the MMSE estimators $\hat{\mathbf{x}}$ and $\hat{\kappa}$ of \mathbf{x} and κ as the posterior mean of $q^k(\mathbf{x})$ and $q^k(\kappa)$, and calculate the estimated support $\hat{\mathcal{S}}$ from $\hat{\mathbf{x}}$.
 - 9: Calculate the extrinsic information based on (17), send $v_{\eta_n \rightarrow s_n}(s_n)$ to SSI Module.
 - 10: **Structured Sparse Inference(SSI) Module:**
 - 11: Perform message passing over the support subgraph \mathcal{G}_B , and send $v_{\phi \rightarrow s_n}(s_n)$ to SC-VBI Module to update the estimated support $\hat{\mathcal{S}}$.
 - 12: **Grid Estimation(GE) Module:**
 - 13: Given fixed $\hat{\mathbf{x}}$, $\hat{\mathcal{S}}$ and, $\hat{\kappa}$, construct the logarithmic likelihood function of $\boldsymbol{\theta}$ using (14).
 - 14: Obtain the ML estimator $\hat{\boldsymbol{\theta}}$ of $\boldsymbol{\theta}$ by performing the gradient update (15) for B_θ times.
 - 15: **end for**
 - 16: **Output** $\hat{\mathbf{x}}$ and $\hat{\boldsymbol{\theta}}$.
-

E. Comparison with Existing Algorithms

We compare the proposed SC-VBI with three state-of-the-art CS-based algorithms, Turbo-CS [7], Turbo-VBI [9], and IF-VBI [14]. Both Turbo-CS and Turbo-VBI involve a matrix inverse each iteration, whose complexity is $\mathcal{O}(N^3)$ per iteration. Although the IF-VBI algorithm has completely avoided any matrix inverse by using the MM method, an additional SVD operation is added. In the proposed SC-VBI, we constrain the matrix inverse in the subspace of the estimated support, which helps to accelerate the convergence speed and improves the convergence accuracy. Moreover, the gradient update in (36) in the SC-VBI uses backtracking line search to find a better step size.

Table I compares the complexity order of different CS-based algorithms. The complexity order of the proposed SC-VBI is among the lowest, i.e., $\mathcal{O}\left(I\left(NM + |\hat{\mathcal{S}}|^3\right)\right)$. Due to the aforementioned advantages of SC-VBI, simulations show that SC-VBI can achieve a much better tradeoff between complexity per iteration, convergence speed, and performance compared to state-of-the-art baselines.

V. SIMULATIONS

In this section, we use the massive MIMO channel estimation problem described in Section II as an example to

Table II: Complexity order of different algorithms, where I represents the iteration number.

Algorithms	Complexity order
Turbo-CS	$\mathcal{O}(IN^3 + N^2M)$
VBI	$\mathcal{O}(IN^3 + N^2M)$
IF-VBI	$\mathcal{O}(N^3 + INM)$
SC-VBI	$\mathcal{O}\left(I\left(NM + \hat{\mathcal{S}} ^3\right)\right)$

demonstrate the advantages of the proposed AE-SC-VBI algorithm. The baseline algorithms considered in the simulations are described below.

- **EM-based Turbo-VBI (EM-Turbo-VBI)** [9], [10]: The E-step is the Turbo-VBI algorithm and the M-step performs gradient ascent update.
- **EM-based Turbo-IF-VBI (EM-Turbo-IF-VBI)** [13]: The E-step is the low complexity Turbo-IF-VBI algorithm without matrix inverse, and the M-step performs gradient ascent update.
- **EM-based Turbo-CS (EM-Turbo-CS)** [7], [8]: The E-step is the Turbo-CS algorithm, and the M-step performs gradient ascent update.

A. Implementation Details

In the simulations, the BS is equipped with a UPA consisting of $N_x = 32$ horizontal antennas and $N_y = 72$ vertical antennas, for a total of $N_r = 2304$ antennas. Define the compression ratio as $\frac{N_r}{N_{RF}}$. The number of azimuth AoA grid points is set to $N_1 = 32$ and the number of elevation AoA grid points is set to $N_2 = 18$, since the elevation angle has a prior range between $-\frac{1}{6}\pi$ and 0 in practical systems. The pilot symbol u is generated with a random phase under unit power constraint. We consider a narrowband multi-path channel generated by 3GPP TR 38.901 model [23]. The normalized mean square error (NMSE) is used as the performance metric for channel estimation. All the algorithms use the 2D-Markov structured prior model without special announcement.

B. Convergence Behavior

In Fig. 7, we compare the convergence behavior of different methods in terms of channel estimation NMSE, we set SNR = 10 dB and the compression ratio is 4. Since the AE-SC-VBI algorithm updates all variables at the same timescale in an alternative way, while the other three baseline algorithms update the dynamic grid at a slower timescale, the AE-SC-VBI converges significantly faster than the other algorithms. Moreover, even for fixed grid, AE-SC-VBI still converges much faster than EM-Turbo-IF-VBI because of the introduction of the subspace constrained matrix inverse. After convergence, the steady-state performance of each algorithms is similar, which indicates that the AE-SC-VBI can accelerate the convergence speed while achieving comparable performance with state-of-the-art methods.

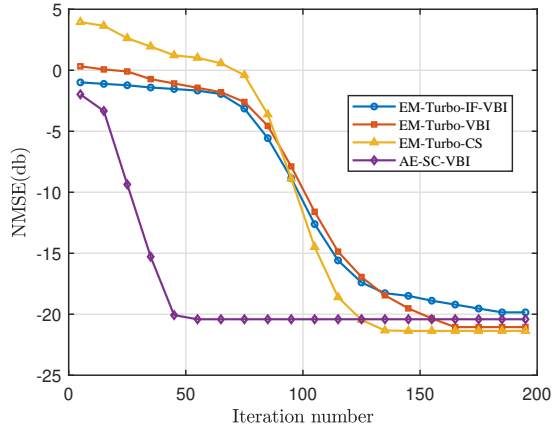


Figure 7: NMSE of channel estimation versus the iteration number.

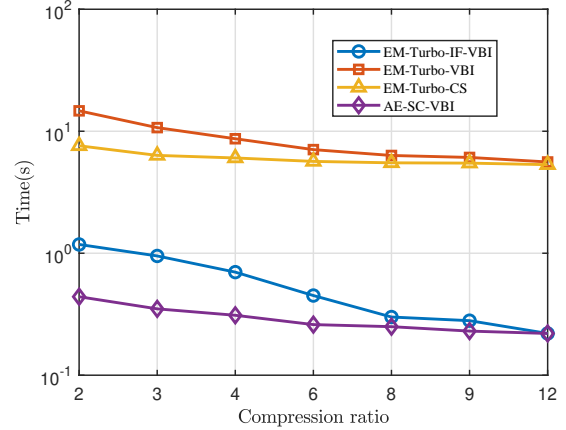


Figure 9: CPU time versus the compress ratio

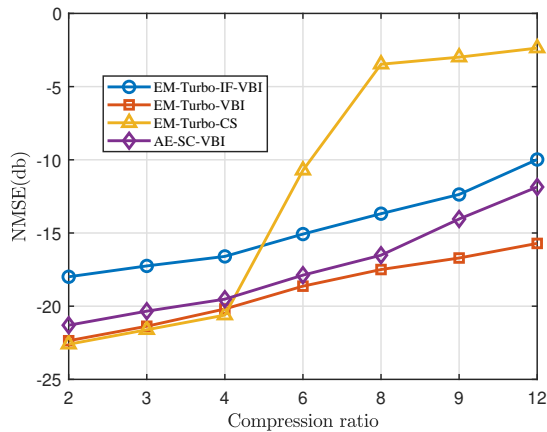


Figure 8: NMSE of channel estimation versus the compress ratio

C. Influence of Number of RF Chains

In Fig. 8, we compare the NMSE performance versus compression ratios when $\text{SNR} = 10$ dB. To show that AE-SC-VBI can achieve a better performance than EM-Turbo-IF-VBI and meanwhile consumes less computing power, the total iteration time of EM-Turbo-IF-VBI is set to be slightly greater than AE-SC-VBI. In Fig. 9, we measure the CPU time of each algorithm in different compression ratios via MATLAB on a laptop computer with a 2.5 GHz CPU.

It can be observed that the CPU time of EM-Turbo-CS and EM-Turbo-VBI is significantly higher than that of EM-Turbo-IF-VBI and AE-SC-VBI, and the CPU time of AE-SC-VBI is significantly lower than that of EM-Turbo-IF-VBI when the compression ratio is low, because the SVD in EM-Turbo-IF-VBI has a higher complexity at low compression ratios. Besides, although the EM-Turbo-CS algorithm has a good performance at low compression ratios, its performance significantly degrades when the compression ratio exceeds 4. As a comparison, the three VBI algorithms can still achieve good performance at high compression ratios. The proposed AE-SC-

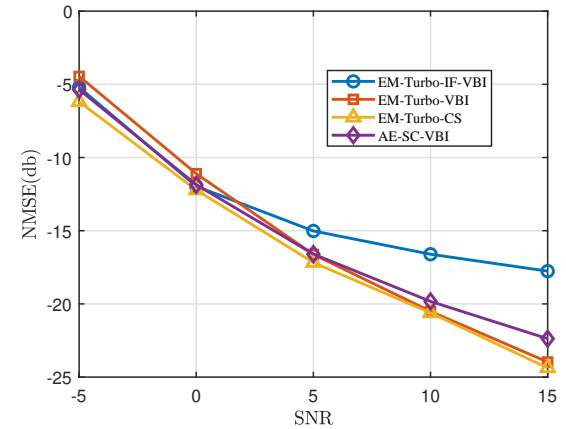


Figure 10: NMSE of channel estimation versus the SNR

VBI algorithm outperforms the EM-Turbo-IF-VBI algorithm at all compression ratios and meanwhile consumes less CPU time. In fact, the performance of AE-SC-VBI algorithm can even approach that of EM-Turbo-VBI who has a much higher complexity order.

D. Influence of SNR

In Fig. 10, we compare the NMSE performance versus SNR, where the compression ratio is set to 4. Our proposed AE-SC-VBI algorithm significantly outperforms the EM-Turbo-IF-VBI algorithm in the high SNR region and has similar performance compared to the high-complexity EM-based Turbo-VBI/Turbo-CS algorithms.

E. Influence of Number of Channel Paths

In Fig. 11, we focus on how the number of channel paths affects the channel estimation performance, where the compression ratio is set to 8 and the SNR is set to 5 dB. It is clear to see that the channel estimation performance of all algorithms gets worse as the number of paths increases.

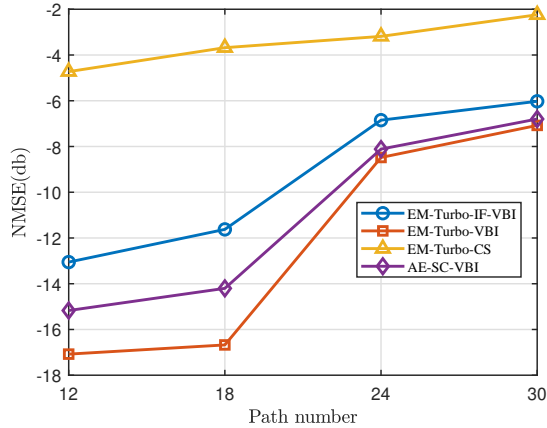


Figure 11: NMSE of channel estimation versus the number of paths.

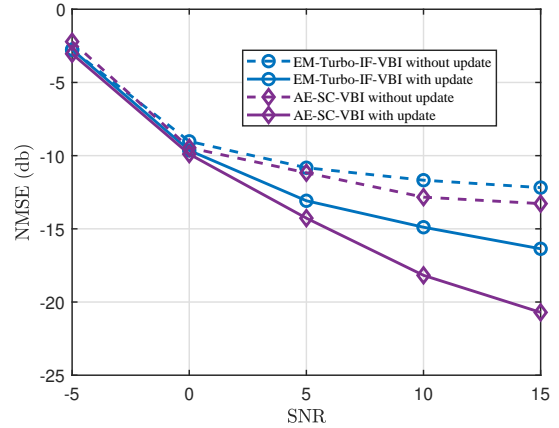


Figure 13: NMSE of channel estimation versus SNR with and without dynamic grid update

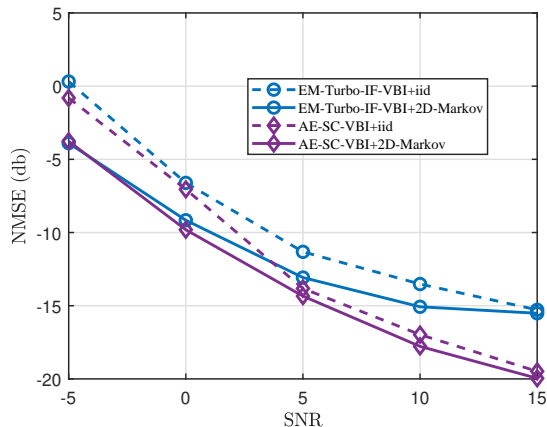


Figure 12: NMSE of channel estimation in different prior model

Due to the compression ratio is larger than 4, the EM-Turbo-CS algorithm works poorly. Again, our proposed AE-SC-VBI achieve a significant performance gain over the EM-Turbo-IF-VBI.

F. Influence of Sparse Prior Model

In Fig. 12, we study the impact of different sparse prior models, i.e, the proposed 2D-Markov prior model and the i.i.d. prior model, where the compression ratio is set to 6. In the low SNR regions, the algorithm with the 2D-Markov prior has a significant performance gain over the same algorithm with an i.i.d. prior. While in the high SNR region, the performance gain becomes relatively small. This is because the observation information is sufficient to estimate the channel well in high SNR regions. In this case, the structured prior information contributes less to the channel estimation performance.

G. Influence of Grid Update

In Fig. 13, we study the impact of dynamic grid update, with the compression ratio set to 6. Our proposed AE-SC-

VBI algorithm updates the grid in the grid estimation module III-A, while the EM-based algorithms update the grid during the M-step. It is clear to see that incorporating dynamic grid update leads to a significant performance improvement in high SNR regions, for both the proposed AE-SC-VBI algorithm and the EM-Turbo-IF-VBI algorithm. Note that since the influence of grid update on the EM-Turbo-VBI and EM-Turbo-CS is similar, their NMSE curves are not shown in Fig. 13 to avoid too many curves in a single plot.

VI. CONCLUSION

We propose an alternating estimation (AE) framework with a novel SC-VBI algorithm (AE-SC-VBI) for robust recovery of structured sparse signals with dynamic grid parameters in the sensing matrix. The AE framework iterates among three modules until convergence: the subspace constrained variational Bayesian inference (SC-VBI) module, the grid estimation (GE) module and the structured sparse inference (SSI) module. For fixed sparse signal from the SC-VBI module, the GE module refines the dynamic grid by directly maximizing the likelihood function based on the gradient ascent method with backtracking line search. For fixed extrinsic message from the SC-VBI module, the SSI module performs sum-product message passing over the structured sparse prior to exploit the specific sparse structures in practical applications. For fixed grid from the GE module and extrinsic message from the SSI module, the SC-VBI module computes a Bayesian estimation of the sparse signal. In the proposed SC-VBI algorithm, the high-dimensional matrix inverse is replaced by a low-dimensional subspace constrained matrix inverse. We further establish the convergence of the SC-VBI to a stationary solution of the KLD minimization problem. Finally, we apply the proposed AE-SC-VBI algorithm to solve a massive MIMO channel estimation problem. The proposed AE-SC-VBI algorithm is shown in the simulations to achieve significant gains over baseline algorithms.

A. Proof of Lemma 2

Given $q(\boldsymbol{\rho})$, $q(\boldsymbol{s})$, $q(\boldsymbol{\kappa})$, the KLD can be calculated as

$$\begin{aligned} \text{KL}(q \parallel p) &= \int q(\mathbf{v}) \ln \frac{q(\mathbf{v})}{\hat{p}(\mathbf{v} | \mathbf{y})} d\mathbf{v} \\ &= \langle \ln q(\mathbf{x}) \rangle_{q(\mathbf{x})} - \langle \ln \hat{p}(\mathbf{v}, \mathbf{y}) \rangle_{q(\mathbf{v})} + C \\ &= \langle \ln q(\mathbf{x}) \rangle_{q(\mathbf{x})} - \langle \ln p(\mathbf{y} | \mathbf{x}, \boldsymbol{\kappa}) \rangle_{q(\mathbf{x})q(\boldsymbol{\kappa})} \\ &\quad - \langle \ln p(\mathbf{x} | \boldsymbol{\rho}) \rangle_{q(\mathbf{x})q(\boldsymbol{\rho})} + C, \\ &= \langle \ln q(\mathbf{x}) \rangle_{q(\mathbf{x})} - \langle \boldsymbol{\kappa} \rangle \left\langle \|\mathbf{y} - \mathbf{A}\mathbf{x}\|^2 \right\rangle_{q(\mathbf{x})} \boldsymbol{\mu}^H \\ &\quad - \langle \mathbf{x}^H \text{diag}(\langle \boldsymbol{\rho} \rangle) \mathbf{x} \rangle_{q(\mathbf{x})} + C, \end{aligned} \quad (39)$$

where C is a constant. Based on the constraint in (23), Problem \mathcal{A}_{VBI} is equivalent to finding the optimal parameters of $q(\mathbf{x})$, denoted by $\{\tilde{\boldsymbol{\mu}}, \tilde{\boldsymbol{\sigma}}^2\}$, so that the KLD in (39) is minimized. The equivalent optimization problem is formulated as

$$\begin{aligned} \tilde{\boldsymbol{\mu}}, \tilde{\boldsymbol{\sigma}}^2 &= \min_{\mathbf{u}, \boldsymbol{\sigma}^2} \left[- \sum_{n=1}^N \ln \sigma_n^2 - \boldsymbol{\mu}^H \text{diag}(1/\boldsymbol{\sigma}^2) \boldsymbol{\mu} \right. \\ &\quad \left. - \left\langle (\mathbf{x} - \boldsymbol{\mu})^H \text{diag}(1/\boldsymbol{\sigma}^2) (\mathbf{x} - \boldsymbol{\mu}) \right\rangle_{q(\mathbf{x})} \right. \\ &\quad \left. + \langle \boldsymbol{\kappa} \rangle \left\langle \|\mathbf{y} - \mathbf{A}\mathbf{x}\|^2 \right\rangle_{q(\mathbf{x})} + \langle \mathbf{x}^H \text{diag}(\langle \boldsymbol{\rho} \rangle) \mathbf{x} \rangle_{q(\mathbf{x})} \right] \\ &= \min_{\mathbf{u}, \boldsymbol{\sigma}^2} \left[- \sum_{n=1}^N \ln \sigma_n^2 - \boldsymbol{\mu}^H \text{diag}(1/\boldsymbol{\sigma}^2) \boldsymbol{\mu} \right. \\ &\quad \left. + \langle \mathbf{x}^H (\mathbf{W} - \text{diag}(1/\boldsymbol{\sigma}^2)) \mathbf{x} \rangle_{q(\mathbf{x})} \right. \\ &\quad \left. - \langle 2\Re \{ \mathbf{x}^H (\mathbf{b} - \text{diag}(1/\boldsymbol{\sigma}^2) \boldsymbol{\mu}) \} \rangle_{q(\mathbf{x})} \right] \\ &= \min_{\mathbf{u}, \boldsymbol{\sigma}^2} \left[- \sum_{n=1}^N \ln \sigma_n^2 - \boldsymbol{\mu}^H \text{diag}(1/\boldsymbol{\sigma}^2) \boldsymbol{\mu} \right. \\ &\quad \left. + \boldsymbol{\mu}^H (\mathbf{W} - \text{diag}(1/\boldsymbol{\sigma}^2)) \boldsymbol{\mu} \right. \\ &\quad \left. + \text{Tr}((\mathbf{W} - \text{diag}(1/\boldsymbol{\sigma}^2)) \text{diag}(\boldsymbol{\sigma}^2)) \right. \\ &\quad \left. - 2\Re \{ \boldsymbol{\mu}^H (\mathbf{b} - \text{diag}(1/\boldsymbol{\sigma}^2) \boldsymbol{\mu}) \} \right] \\ &= \min_{\mathbf{u}, \boldsymbol{\sigma}^2} \left[\mathbf{u}^H \mathbf{W} \mathbf{u} - 2\Re \{ \mathbf{u}^H \mathbf{b} \} + \sum_{n=1}^N (W_n \sigma_n^2 - \ln \sigma_n^2) \right], \end{aligned} \quad (40)$$

which is equal to (26).

B. Proof of Theorem 3

The SC-VBI can be viewed as an alternating optimization method to solve Problem \mathcal{A}_{VBI} . It is clear that the SC-VBI can monotonically decreasing the KLD objective, thus the KLD will converge to a limit. For convenience, we use $\boldsymbol{\xi} \triangleq \{\boldsymbol{\mu}, \boldsymbol{\sigma}^2, \tilde{\mathbf{a}}, \tilde{\mathbf{b}}, \tilde{\boldsymbol{\lambda}}, \tilde{\mathbf{c}}, \tilde{\mathbf{d}}\}$ to represent the parameters of $q(\mathbf{v})$. Let $\boldsymbol{\xi}_j$ denote the j -th block of $\boldsymbol{\xi}$ for $j = 1, \dots, B$, where $B = |\boldsymbol{\xi}|$. Then, the KLD in (21) can be rewritten as a function of $\boldsymbol{\xi}$, i.e.

$$\text{KL}(\boldsymbol{\xi}) = \int q(\mathbf{v}; \boldsymbol{\xi}) \ln \frac{q(\mathbf{v}; \boldsymbol{\xi})}{\hat{p}(\mathbf{v} | \mathbf{y}; \boldsymbol{\xi})} d\mathbf{v}. \quad (41)$$

In the following, we will prove that every limiting point $q^*(\mathbf{v}; \boldsymbol{\xi}^*)$ generated by the SC-VBI is a stationary solution of Problem \mathcal{A}_{VBI} .

In the i -th iteration of the SC-VBI, we update $\boldsymbol{\xi}_j, \forall j$ alternatively as

$$\boldsymbol{\xi}_j^{(i)} \begin{cases} = \text{argmin}_{\boldsymbol{\xi}_j} \text{KL}(\boldsymbol{\xi}_j, \boldsymbol{\xi}_{-j}^{(i-1)}), & \text{if } \boldsymbol{\xi}_j \neq \boldsymbol{\mu}, \\ = \boldsymbol{\mu}^{(i-1)} - \epsilon_x^{(i)} \nabla_{\boldsymbol{\mu}} \text{KL}(\boldsymbol{\mu}, \boldsymbol{\xi}_{-j}^{(i-1)}) |_{\boldsymbol{\mu}=\boldsymbol{\mu}^{(i-1)}}, & \text{if } \boldsymbol{\xi}_j = \boldsymbol{\mu}, \end{cases} \quad (42)$$

where $(\cdot)^{(i)}$ stands for the i -th iteration and $\boldsymbol{\xi}_{-k}^{(i)} = (\boldsymbol{\xi}_1^{(i)}, \dots, \boldsymbol{\xi}_{k-1}^{(i)}, \boldsymbol{\xi}_{k+1}^{(i)}, \dots, \boldsymbol{\xi}^{(i-1)})$. For case of $\boldsymbol{\xi}_j \neq \boldsymbol{\mu}$, it is clear that $\text{KL}(\boldsymbol{\xi}_j, \boldsymbol{\xi}_{-j}^{(i-1)})$ is minimized w.r.t. $\boldsymbol{\xi}_j$. While for case of $\boldsymbol{\xi}_j = \boldsymbol{\mu}$, we have $\text{KL}(\boldsymbol{\mu}^{(i-1)}, \boldsymbol{\xi}_{-j}^{(i-1)}) \geq \text{KL}(\boldsymbol{\mu}^{(i)}, \boldsymbol{\xi}_{-j}^{(i-1)})$ based on the property of gradient update, where the equality holds only when the gradient w.r.t. $\boldsymbol{\mu}$ is zero. Therefore, the KLD will keep decreasing until converging to a certain value, and we must have

$$\lim_{i \rightarrow \infty} \nabla_{\boldsymbol{\xi}_j} \text{KL}(\boldsymbol{\xi}_j, \boldsymbol{\xi}_{-j}^{(i-1)}) = 0, \forall j. \quad (43)$$

(otherwise, the KLD will keep decreasing to negative infinity, which contradicts with the fact that $\text{KL}(\boldsymbol{\xi}) \geq 0$). Then according to (43) and the property of gradient update, we must have $\lim_{i \rightarrow \infty} \|\boldsymbol{\mu}^{(i)} - \boldsymbol{\mu}^{(i-1)}\| = 0$. Moreover, it follows from (43) and the strong convexity of $\text{KL}(\boldsymbol{\xi}_j, \boldsymbol{\xi}_{-j}^{(i-1)})$ w.r.t. $\boldsymbol{\xi}_j, \forall \boldsymbol{\xi}_j \neq \boldsymbol{\mu}$ that $\lim_{i \rightarrow \infty} \|\boldsymbol{\xi}_j^{(i)} - \boldsymbol{\xi}_j^{(i-1)}\| = 0, \forall \boldsymbol{\xi}_j \neq \boldsymbol{\mu}$. Therefore, we have

$$\lim_{i \rightarrow \infty} \|\boldsymbol{\xi}_j^{(i)} - \boldsymbol{\xi}_j^{(i-1)}\| = 0, \forall j. \quad (44)$$

It follows from (44) that all the B sequences $\{\boldsymbol{\xi}_j^{(i)}, \boldsymbol{\xi}_{-j}^{(i)}\}, j = 0, 1, \dots, B-1$ have the same set of limiting points. Let $\{\boldsymbol{\xi}_j^{(i_t)}, \boldsymbol{\xi}_{-j}^{(i_t)}, t = 1, 2, \dots\}$ denote a subsequence that converges to a limiting point $\boldsymbol{\xi}^*$. Suppose $\boldsymbol{\xi}^*$ is not a stationary point of $\text{KL}(\boldsymbol{\xi})$, then $\nabla_{\boldsymbol{\xi}} \text{KL}(\boldsymbol{\xi}) \neq 0$ and it follows from (44) that $\lim_{t \rightarrow \infty} \nabla_{\boldsymbol{\xi}_j} \text{KL}(\boldsymbol{\xi}_j, \boldsymbol{\xi}_{-j}^{(i_t)}) \neq 0$ must hold at least for some j , which contradicts with (43). Therefore, every limiting point $\boldsymbol{\xi}^*$ must be a stationary point of $\text{KL}(\boldsymbol{\xi})$. In other word, every limiting point $q^*(\mathbf{v}; \boldsymbol{\xi}^*)$ generated by the SC-VBI is a stationary solution of Problem \mathcal{A}_{VBI} .

REFERENCES

- [1] Z. Yang, L. Xie, and C. Zhang, "Off-grid direction of arrival estimation using sparse Bayesian inference," *IEEE Trans. Signal Process.*, vol. 61, no. 1, pp. 38–43, 2013.
- [2] C. Zhou, Y. Gu, X. Fan, Z. Shi, G. Mao, and Y. D. Zhang, "Direction-of-arrival estimation for coprime array via virtual array interpolation," *IEEE Trans. Signal Process.*, vol. 66, no. 22, pp. 5956–5971, 2018.
- [3] J. Dai, A. Liu, and V. K. N. Lau, "FDD massive MIMO channel estimation with arbitrary 2D-array geometry," *IEEE Trans. Signal Process.*, vol. 66, no. 10, pp. 2584–2599, 2018.
- [4] F. Liu, Y. Cui, C. Masouros, J. Xu, T. X. Han, Y. C. Eldar, and S. Buzzi, "Integrated sensing and communications: Toward dual-functional wireless networks for 6G and beyond," *IEEE J. Sel. Areas Commun.*, vol. 40, no. 6, pp. 1728–1767, 2022.

- [5] C. De Lima, D. Belot, R. Berkvens, A. Bourdoux, D. Dardari, M. Guillaud, M. Isomursu, E.-S. Lohan, Y. Miao, A. N. Barreto, M. R. K. Aziz, J. Saloranta, T. Sanguanpuak, H. Srieddeen, G. Seco-Granados, J. Sutuala, T. Svensson, M. Valkama, B. Van Liempd, and H. Wymeersch, "Convergent communication, sensing and localization in 6G systems: An overview of technologies, opportunities and challenges," *IEEE Access*, vol. 9, pp. 26 902–26 925, 2021.
- [6] S. Som and P. Schniter, "Compressive imaging using approximate message passing and a Markov-tree prior," *IEEE Trans. Signal Process.*, vol. 60, no. 7, pp. 3439–3448, 2012.
- [7] J. Ma, X. Yuan, and L. Ping, "Turbo compressed sensing with partial DFT sensing matrix," *IEEE Signal Process. Lett.*, vol. 22, no. 2, pp. 158–161, 2015.
- [8] A. Liu, L. Lian, V. K. N. Lau, and X. Yuan, "Downlink channel estimation in multiuser massive MIMO with hidden Markovian sparsity," *IEEE Trans. Signal Process.*, vol. 66, no. 18, pp. 4796–4810, 2018.
- [9] A. Liu, G. Liu, L. Lian, V. K. N. Lau, and M.-J. Zhao, "Robust recovery of structured sparse signals with uncertain sensing matrix: A Turbo-VBI approach," *IEEE Trans. Wireless Commun.*, vol. 19, no. 5, pp. 3185–3198, 2020.
- [10] A. Liu, L. Lian, V. Lau, G. Liu, and M.-J. Zhao, "Cloud-assisted cooperative localization for vehicle platoons: A turbo approach," *IEEE Trans. Signal Process.*, vol. 68, pp. 605–620, 2020.
- [11] L. Lian, A. Liu, and V. K. N. Lau, "Exploiting dynamic sparsity for downlink FDD-massive MIMO channel tracking," *IEEE Trans. Signal Process.*, vol. 67, no. 8, pp. 2007–2021, 2019.
- [12] Z. Huang, K. Wang, A. Liu, Y. Cai, R. Du, and T. X. Han, "Joint pilot optimization, target detection and channel estimation for integrated sensing and communication systems," *IEEE Trans. Wireless Commun.*, vol. 21, no. 12, pp. 10 351–10 365, 2022.
- [13] H. Duan, L. Yang, J. Fang, and H. Li, "Fast inverse-free sparse Bayesian learning via relaxed evidence lower bound maximization," *IEEE Signal Process. Lett.*, vol. 24, no. 6, pp. 774–778, 2017.
- [14] W. Xu, Y. Xiao, A. Liu, M. Lei, and M.-J. Zhao, "Joint scattering environment sensing and channel estimation based on non-stationary Markov random field," *IEEE Trans. Wireless Commun.*, vol. 23, no. 5, pp. 3903–3917, 2024.
- [15] W. Xu, A. Liu, B. Zhou, and M.-j. Zhao, "Successive linear approximation VBI for joint sparse signal recovery and dynamic grid parameters estimation," [Online]. Available: <https://arxiv.org/pdf/2307.09149>.
- [16] G. Tang, B. N. Bhaskar, P. Shah, and B. Recht, "Compressed sensing off the grid," *IEEE Trans. Inf. Theory*, vol. 59, no. 11, pp. 7465–7490, 2013.
- [17] Z. Yang and L. Xie, "Enhancing sparsity and resolution via reweighted atomic norm minimization," *IEEE Trans. Signal Process.*, vol. 64, no. 4, pp. 995–1006, 2016.
- [18] D. G. Tzikas, A. C. Likas, and N. P. Galatsanos, "The variational approximation for Bayesian inference," *IEEE Signal Process. Mag.*, vol. 25, no. 6, pp. 131–146, 2008.
- [19] Y. Wan and A. Liu, "A two-stage 2D channel extrapolation scheme for tdd 5G NR systems," *IEEE Trans. on Wireless Commun.*, pp. 1–1, 2024.
- [20] A. Liu, V. K. N. Lau, and W. Dai, "Exploiting burst-sparsity in massive MIMO with partial channel support information," *IEEE Trans. Wireless Commun.*, vol. 15, no. 11, pp. 7820–7830, 2016.
- [21] E. Fornasini, "2D Markov chains," *Linear Algebra Appl.*, vol. 140, pp. 101–127, 1990.
- [22] F. Kschischang, B. Frey, and H.-A. Loeliger, "Factor graphs and the sum-product algorithm," *IEEE Trans. Inf. Theory*, vol. 47, no. 2, pp. 498–519, 2001.
- [23] E. Endovitskiy, A. Kureev, and E. Khorov, "Reducing computational complexity for the 3GPP TR 38.901 MIMO channel model," *IEEE Wireless Commun. Letters*, vol. 11, no. 6, pp. 1133–1136, 2022.